arXiv:1512.05142v1 [physics.plasm-ph] 16 Dec 2015

Reflected attosecond pulse radiation from moving electron layers

Mykyta Cherednychek and Alexander Pukhov
Institut für theoretische Physik, Heinrich-Heine-Universität Düsseldorf

(Dated: December 17, 2015)

With the generation of high order harmonics (HHG) on the plasma surface it is possible to turn the laser pulse into a train of attosecond or even zeptosecond pulses in the back radiation. These attosecond pulses may have amplitude several orders of magnitude larger than that of the laser pulse under appropriate conditions. We study this process in detail, especially the nanobunching of the plasma electron density. We derive the analytical expression that describes the electron density profile and obtain a good agreement with particle-in-cell simulations. We investigate the most efficient case of HHG at moderate laser intensity ($a_0 = 10$) on the over dense plasma slab with an exponential profile per-plasma. Subsequently we calculate the spectra of single attosecond pulses from back radiation using our expression for density shape in combination with the equation for spectrum of nanobunch radiation.

INTRODUCTION

The development of laser technology showed an immense progress in last decade [1–4]. This progress offers an opportunity to study the new physics phenomena of laser plasma interaction. One of the most important processes in this field is the generation of high order harmonics (HHG), which is studied very intensely today. As the minimum achievable duration of laser pulses was reducing with time, it is interesting whether the generation even shorter pulses (in attosecond or even zeptosecond range) is possible. The reduction of the pulse duration and the radiation wavelength would open new potential applications. This is the motivation of the investigation of HHG. The most efficient method of HHG is the interaction process of the high contrast laser pulses [5] with solid density targets. The pedestal of the pulse ionizes the surface and the main pulse interacts with overdense plasma electrons, while ions remain nearly immobile during the short pulse duration. One distinguishes two main HHG mechanisms in this case: coherent wake emission (CWE) [5, 6] and "relativistically oscillating mirror" (ROM) [7–11]. CWE is caused by fast Brunel electrons [12] which excite the plasma oscillations at the local plasma frequencies. Thus there is no harmonics behind the maximal plasma frequency in the case of CWE. This process dominates for non-relativistic laser intensities $a_0 \lesssim 1$. For $a_0 \gg 1$ the harmonics are generated mostly via ROM. In this case the electron layer at the plasma surface acts as a mirror that oscillates at relativistic velocities and generates high order harmonics via Doppler effect moving toward the incident wave. By this process there is no limit of frequency like by CWE, so higher harmonics can be generated. The first theoretical description of ROM claimed that the intensity spectrum envelope of reflected wave can be described by $I(n) \propto n^{-5/2}$ until "roll over" frequency ω_r proportional to $4\gamma^2$, where n is the harmonic order and γ is the relativistic gamma factor [7]. Later this theory was improved, especially the acceleration of the reflecting layer was taking into account. This results to the power law $I(n) \propto n^{-8/3}$ and $\omega_r \propto \gamma^3$ [8]. This model assumes the existence of so called apparent reflection point (ARP) where the transverse electric field vanishes. This model was experimentally proved [9–11]. Most recently another HHG mechanism was discovered. Using p-polarized oblique incident pulse with $a_0 \gg 1$ one can cause the formation of extremely dense electron nanobunches under appropriate conditions. These bunches irradiate attosecond pulses with intensities much larger comparing to incident pulse [13, 14]. That means that the boundary condition assumed in [8] corresponding to ARP fails and thus the ROM theory can't be applied in this case. This process is called coherent synchrotron emission (CSE). The reflected radiation in case of CSE in characterized by the power law $I(n) \propto n^{-4/3}$ or $I(n) \propto n^{-6/5}$ which is flatter comparing to ROM [13, 14]. The corresponding experiments can be found in Ref. [15–17]. Detailed numerical investigation of the case of p-polarized oblique incidence in Ref. [18] figures out that the ROM model can be violated when the similarity parameter $S = n/a_0$ (where n is the electron density given in units of the critical density n_c and a_0 is the dimensionless laser amplitude [19]) is smaller than five. The authors of [18] present a new relativistic electronic spring (RES) model for $S > 5$.

PIC simulation of the HHG process

For our simulations we use one dimensional version of PIC code called Virtual Laser Plasma Laboratory [20]. In our geometry the incident wave comes from the left hand side of the simulation box and propagates along x-axis. The wave is p-polarized and the electric field component oscillates along the y-axis. The plasma is located at the right hand side of simulation box. It is also possible to describe the interactions where oblique incidence is used with our code. Let θ be the angle of incidence in labora-

tory frame and consider some frame moving along y-axis with velocity $V = c\sin\theta$. Lorenz transformations verify that in this frame the laser is normally incident (see [21] for more details). At the same time the whole plasma moves in y-direction in this frame. Thus, attributing some initial velocity to plasma in our simulation we are working in the moving frame. If we need the results in laboratory frame, we have to transform the values obtained from the simulation via Lorenz transformation. Consequently we obtain results that correspond to the process with oblique incidence. We use the incident field $E_i(t)$ of duration $T = 10\lambda/c$, that is given by

$$E_i(t) = \frac{1}{4}\left(1+\tanh\left(\frac{t}{\Delta t}\right)\right) \times \left(1-\tanh\left(\frac{t-T}{\Delta t}\right)\right)\sin(2\pi t),$$

where $\Delta t = \lambda/4$. Further we use the plasma exponential density ramp for $x < 0$. For $x > 0$ density remains constant.

$$n(x) = \begin{cases} n_0 e^{\frac{x}{\sigma}} & \text{for} \quad x < 0 \\ n_0 & \text{for} \quad x > 0 \end{cases}. \tag{1}$$

Assuming that the ions are at rest during the whole interaction process we consider only the interaction between the electrons and the incident wave. In the simple case of normal incidence there are two forces acting on particles along x-axis. The electrostatic force proportional to E_x and laser ponderomotive force oscillating with 2ω (twice of the laser frequency). Thus the plasma surface oscillates with the half of the laser period. In the case of oblique incidence of p-polarized wave there is additional longitudinal component of the electric field oscillating at frequency ω and acting on surface. Consequently the interaction becomes even more complicated which leads to stronger oscillations on plasma surface containing both ω and 2ω mods.

As we can see as soon as the electrons are puled back by the electrostatic force they form a thin nanobunch that reaches velocity close to c. In this case the generation of high harmonics is possible.

DENSITY PROFILE OF A THIN ELECTRON LAYER

In this section we derive two different analytic expressions for two different cases, which roughly describe the electron density profile at the intervals where the sharp spikes appear. The starting point of our calculations is the approximation of the electron phase space distribution at these intervals. As we will see later this distribution depends on the propagation velocity $\dot{x}_0(t)$ of given electron layer.

Firstly let us consider the case of slow $\dot{x}_0(t) \ll c$ electron bunch. In Fig. 1 the electron density and its distribution in x-p_x-phase space at a certain time are visualized. Let's claim that the curve in phase space is described by the function $x(p)$ at some small interval close to the density spike. Obviously, x_0 is the local minimum of this function that coincides with the position of the spike. In fact, we have always a spike of electron density at the point, where the function $x(p)$ exhibits the local extreme value. The idea that gives us the staring point for our calculations is the following. We can locally describe the given curve in phase space as a parabola:

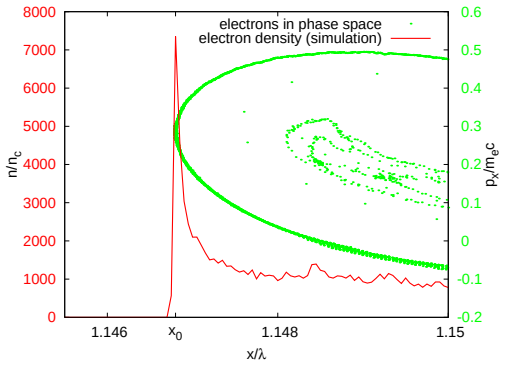

FIG. 1: Electron density (red) and electrons in x-p_x-plane (green). x_0 is the position of the maximal density. Simulation parameters: initial plasma density $n_0 = 38.9n_c$; $\sigma = 1.1836 \cdot 10^{-3}\lambda$(Laboratory frame), Pulse with dimensionless amplitude $a_0 = 10$ and p-polarized oblique incidence at 57° angle has the wave length $\lambda = 820$nm.

$$x(p,t) = x_0(t) + \alpha(t)(p - p_0(t))^2. \tag{2}$$

The point $(x_0(t),\ p_0(t))$ corresponds to the local minimum. In order to simplify the notation, we drop the time dependence and set $p_0 = x_0 = 0$. Then we have

$$x(p) = \alpha p^2.$$

We consider some short interval Δx where this assumption makes sense. The distribution function of the electrons is then given by

$$f_a(x,p) = \mathcal{C}\delta_a\left(x - \alpha p^2\right), \tag{3}$$

where $\mathcal{C}$ is a normalization constant and δ_a is defined as

$$g_a(x) \equiv \frac{3}{4a}\left(1 - \frac{x^2}{a^2}\right)$$
$$\delta_a(x) \equiv \begin{cases} g_a(x) & \text{for} \quad x \in [-a,a] \\ 0 & \text{otherwise} \end{cases},$$

with the property

$$\lim_{a\to 0}\delta_a(x) = \delta(x). \tag{4}$$

The parameter a describes the width of δ_a, which means that $a > 0$ is required. In order to get the expression of density we have to perform the integration in momentum space

$$n_a(x) = \int dp f_a(x,p). \tag{5}$$

We have to be careful with integration boundaries since δ_a is the bounded support function. As a result we obtain:

$$n_a(x) = \begin{cases} \frac{2\mathcal{C}}{5a^3\sqrt{\alpha}}\left(3a^2 - 2x^2 + ax\right)\sqrt{x+a} & \text{for} \quad x \in [-a, a] \\ \frac{2\mathcal{C}}{5a^3\sqrt{\alpha}}\Big(\left(3a^2 - 2x^2\right)\left(\sqrt{x+a} - \sqrt{x-a}\right) \\ \qquad + ax\left(\sqrt{x+a} + \sqrt{x-a}\right)\Big) & \text{for} \quad x > a \\ 0 & \text{for} \quad x < -a. \end{cases} \tag{6}$$

In order to calculate the constant $\mathcal{C}$, we first write an equation for the number of particles in the interval $[-a : \Delta x]$ bei integrating the density on this interval

$$N_{a,\Delta x} = \mathcal{C}\int_{-a}^{\Delta x} dx\; n_a(x) \overset{a \ll \Delta x}{=} 2\mathcal{C}\sqrt{\frac{\Delta x}{\alpha}}. \tag{7}$$

Further we solve the obtained equation for $\mathcal{C}$ and insert it into equation (6). Finally we obtain the expression for electron density profile

$$n_a(x) = \begin{cases} \frac{N_{a,\Delta x}}{5a^3\sqrt{\Delta x}}\left(3a^2 - 2x^2 + ax\right)\sqrt{x+a} & \text{for} \quad x \in [-a, a] \\ \frac{N_{a,\Delta x}}{5a^3\sqrt{\Delta x}}\Big(\left(3a^2 - 2x^2\right)\left(\sqrt{x+a} - \sqrt{x-a}\right) \\ \qquad + ax\left(\sqrt{x+a} + \sqrt{x-a}\right)\Big) & \text{for} \quad x > a \\ 0 & \text{for} \quad x < -a. \end{cases} \tag{8}$$

Note that the parameter α cancels, so it doesn't affect the density profile. In Fig. 2 we see that the density described with (8) agrees very well with simulation results. We call the case where $\dot{x}_0(t) \ll c$ is valid "parabolic case". We chose quite a small value for a because we are dealing with a very big and sharp spike in this example. This is the case since we use a strong laser pulse and very small cell size ($5 \cdot 10^{-5}\lambda$).

Now we discuss another case with $\dot{x}_0(t) \to c$. Consider the phase space evolution taken from the other simulation illustrated in Fig. 3. At the beginning by $t = 5.4\lambda/c$ the momentum is close to zero and the distribution is

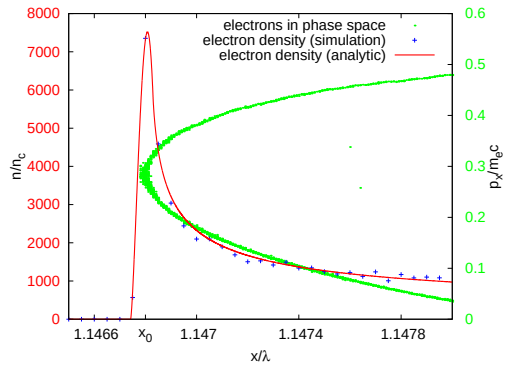

FIG. 2: Electron density taken from the simulation (blue) and calculated analytically via (8) (red), with same simulation parameters compared to Fig. 1, $\Delta x = 0.0012\lambda$; $a = 4.4 \cdot 10^{-5}$ (simulation frame).

parabolic as expected. Further, as soon as the electron bunch is puled back by the electrostatic force, the negative momentum of the bunch growth constantly with time and the distribution changes reminding a kind of "whip" between $t = 5.7\lambda/c$ and $t = 5.8\lambda/c$. The extremely dense electron nanobunch reaches the velocity close to c during this period. In this case the phase space distribution can

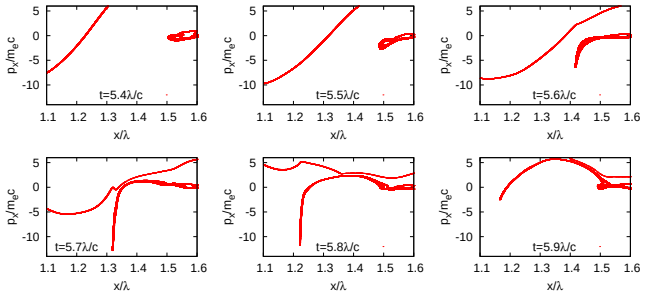

FIG. 3: Electrons in x-p_x-plane taken from the simulation to different times t during the process of nanobunching. Simulation parameters: initial plasma density $n_0 = 100n_c$; $\sigma = 0.4\lambda$ (laboratory frame), Pulse with dimensionless amplitude $a_0 = 10$ and p-polarized oblique incidence at 50° angle has the wave length $\lambda = 820$nm.

be roughly fitted with an exponential function

$$x_p(p,t) = x_0(t) + e^{\alpha(t)(p - p_0(t))}. \tag{9}$$

As we will show later the incident angle and the density gradient used here are optimal for producing the most intense attosecond pulse. Given phase space distribution belongs to the nanobunch that radiates this pulse. Like in the previous case we drop the time dependence and set $p_0 = x_0 = 0$. Then we have

$$x_p(p) = e^{\alpha p} \tag{10}$$

and the distribution function:

$$f_a(x,p) = \mathcal{C}\delta_a\left(x - e^{\alpha p}\right). \tag{11}$$

The density can be given by

$$n_a(x) = \int_{-p_{\rm cut}} dp f_a(x,p) \tag{12}$$

in this case, since we should take into account that the momentum of the electrons is limited by some amount $p_{\rm cut}$. Further we calculate the number of particles on some interval $[x_{\rm min} : x_{\rm max}]$, where $x_{\rm min} = e^{-\alpha p_{\rm cut}}$, in order to obtain $\mathcal{C}$. Finally we calculate:

$$n_a(x) = \begin{cases} \dfrac{3N}{4a^3 \ln\left(\frac{x_{\rm max}}{x_{\rm min}}\right)} \\ \times\left((x+a)\left(x+(x-a)\left(\dfrac{1}{2}+\ln\left(\dfrac{x_{\rm min}}{x+a}\right)\right)\right)\right. \\ \left. + x_{\rm min}\left(\dfrac{1}{2}x_{\rm min} - 2x\right)\right) & \text{for } x \in [x_{\rm min}-a, x_{\rm min}+a] \\ \dfrac{3N}{4a^3 \ln\left(\frac{x_{\rm max}}{x_{\rm min}}\right)} \\ \times\left(2ax - (x^2-a^2)\ln\left(\dfrac{x+a}{x-a}\right)\right) & \text{for } x > x_{\rm min}+a \\ 0 & \text{for } x < x_{\rm min}-a \end{cases} \tag{13}$$

Now as in the previous case we are going to compare the calculated analytical function with the simulated density profile (Fig. 4). Again we obtain a good agreement

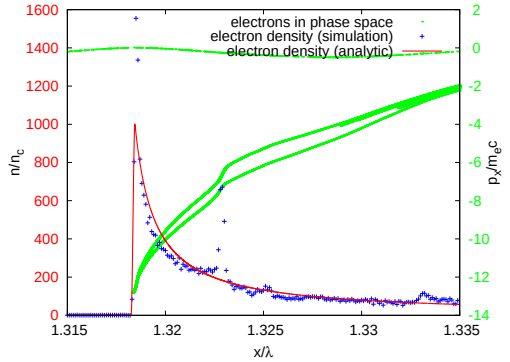

FIG. 4: Electron density taken from simulation (blue) and calculated analytically via (13) (red), as well as electrons in x-p_x-plane (green), with same simulation parameters compared to Fig. 3, taken at $t = 5.7\lambda/c$. $x_{\rm min} - x_0 = 9 \cdot 10^{-4}\lambda$; $x_{\rm max} - x_0 = 0.02\lambda$; $a = 1 \cdot 10^{-4}$ (simulation frame).

and are able to describe the density spike quite well.

Before we go further to the next chapter we analyze the intermediate case $\dot{x}_0(t) \lesssim c$, which is important for further application. In this case the electron phase space distribution looks like its shown in Fig. 5 and can't be approximated well either with parabolic nor with exponential function. Nevertheless we find out that the density profile of the spike can still be well approximated with equation (8) (Fig. 5), so we classify the cases with intermediate velocities as parabolic.

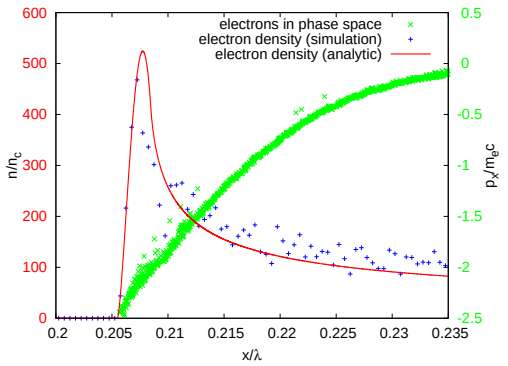

FIG. 5: Electron density taken from simulation (blue) and calculated analytically via (8) (red), as well as electrons in x-p_x-plane (green). Simulation parameters: initial plasma density $n_0 = 100n_c$; $\sigma = 0.066\lambda$ (laboratory frame), Pulse with dimensionless amplitude $a_0 = 10$ and p-polarized oblique incidence at 60° angle has the wave length $\lambda = 820$nm.

In the following chapter we are going to analyze corresponding simulation results more extensively. We will use the descriptions of the electron layer density profile derived here in order to calculate an expression for the spectra of the reflected waves in different cases.

ELECTRON DENSITY EVOLUTION AND HHG EMISSION

We are interested in high frequency spectrum of the reflected pulse mostly determined by the behavior of the ARP when it moves away from plasma with maximal velocity. This moment corresponds to a stationary phase point (SPP) (see [13, 14]). The ARP gamma factor exhibits a sharp spike in this time, it is called γ-spike [8]. One distinguish different orders of γ-spikes depending on behavior of the transverse current in vicinity of SPP, which can by approximated with

$$j_\perp(t,x) \approx (-\alpha_0 t)^n f(x - x_0(t)). \tag{14}$$

We assume that the transverse current density doesn't change its shape f during the time. The number n denotes order of the given γ-spike. The reflected radiation is determined by the transverse current distribution via

$$E_r(t) = \pi \int j_\perp(t-x,x)dx, \tag{15}$$

so we are able to derive the expression for the spectrum of the reflected pulse in line with [13, 14] and obtain:

$$I(\omega) = 4\pi^4 \alpha_0^2 (\alpha_1 \omega)^{-\frac{2n+2}{2n+1}} \left(\frac{d^n}{d\xi^n} Ai_n(\xi_n) \right)^2 |f(\omega)|^2, \quad (16)$$

$$\xi_n = \alpha_1^{-\frac{1}{2n+1}} \delta \omega^{\frac{2n}{2n+1}}, \quad Ai_n = \frac{1}{2\pi} \int e^{i\left(xt + \frac{t^{2n+1}}{2n+1}\right)} dt,$$

$$\alpha_1 = \frac{a_0^2}{2\upsilon n_m^2}, \quad \delta = 1 - \upsilon,$$

where υ is the maximal velocity of the moving electron layer in SPP and n_m the maximal density assumed to be constant in time. In (15) we use the normalized PIC units, see [22] for more detail. To give the expression for the shape function we use the results from the previous section and write

$$f(x) = \frac{n_a(x)}{n_a(x_\mathrm{m})} e^{-\frac{x^2}{\tilde{\sigma}^2}}, \quad n_a(x_\mathrm{m}) = n_m. \quad (17)$$

We multiply the density profile with wider Gaussian function since n_a decays too slowly ($\propto 1/x$ whip or $\propto 1/\sqrt{x}$ parabolic) for positive x and after certain x-value doesn't coincide with given density.

Further we consider two different examples were we apply (16) to calculate the spectrum of the single reflected pulse $E_r^{\mathrm{pls}}(t)$, that is filtered out by the Gaussian function

$$E_r^{\mathrm{pls}}(t) = E_r(t) e^{(t-t_{\max})^2/\tilde{\sigma}^2}, \quad (18)$$

where $t_{\max}$ corresponds to the maximal wave amplitude and $\tilde{\sigma} = 0.2\lambda/c$.

At first we investigate the example of the whip case ($\dot{x}_0(t) \to c$) from the previous section illustrated in Fig. 3 and Fig. 4 more extensively. The electron nanobunch which radiates strong attosecond pulse can be clearly recognized from Fig. 6 and 7 (a). For convenience we chose

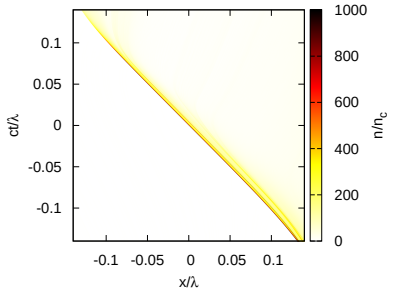

FIG. 6: The electron density distribution of the radiating nanobunch in space time domain. Simulation parameters are the same compared to Fig. 3. The SPP (here (0,0)) corresponds to $t = 5.7\lambda/c$ as in Fig. 4.

the coordinates in the way that the SPP is in the point (0,0). In Fig. 8 (b) the spectrum calculated using (16) is

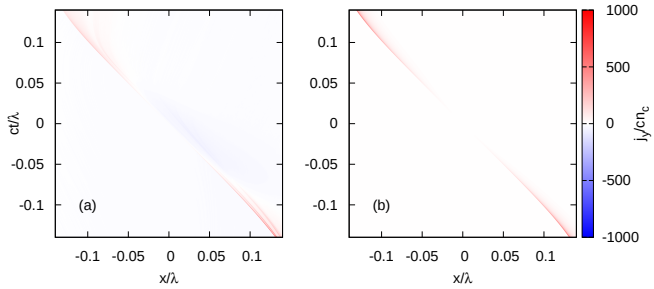

FIG. 7: Transverse current density from the simulation near the SPP (0,0) (a) and calculated analytically via. (14), $n = 2$ (b). Simulation parameters are the same compared to Fig. 3. The parameters used by the analytical calculation for $x_0(t)$: $\alpha_0 = 4 \cdot 10^4$, $n_\mathrm{m} = 1000$ and $\gamma = 15$, for shape: $a = 1 \cdot 10^{-4}\lambda$, $x_{\min} = 9 \cdot 10^{-4}\lambda$ and $\tilde{\tilde{\sigma}} = 0.02\lambda$. The velocity υ is derived from the given gamma factor. The Fourier transform of the shape function $f(\omega)$ is calculated numerically using FFT.

compared with the spectrum calculated von original reflected Pulse via FFT. Obviously, the description works well almost until 1000-th harmonic. In Fig. 8 (a) the

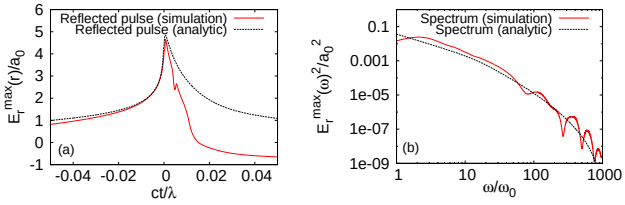

FIG. 8: Reflected radiation obtained from the simulation ((a) red) and from analytical current distribution ((a) black), as well as the corresponding spectra in (b). The spectrum from the simulation is taken directly from the radiated pulse via FFT, while the other one is obtained using the equation (16).

corresponding pulses are compared. The both graphs behave in the similar manner.

Going along the same lines we analyze now the intermediate case $\dot{x}_0(t) \lesssim c$ shown in Fig. 5. Es we said before we attribute this case to the parabolic case. The corresponding pictures illustrating this case are Fig. 9, 10 and 11. Here the velocity in SPP significantly deviates from the speed of light and approximately equals to $0.91c$. For that reason the electron phase space distribution doesn't become "whip-like" (Fig. 5). Although there is no ultrarelativistic regime here, we still may apply the same analysis assuming the absolute velocity of the electrons to be approximately constant close to SPP. Again we obtain good agreement for the spectrum behavior.

We see that in the first example (whip case) we have the second order gamma spike, whether in the second

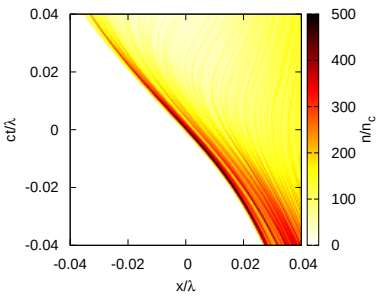

FIG. 9: The electron density distribution of the radiating nanobunch the in space time domain. Simulation parameters are the same compared to Fig. 5. The density profile in SPP (here (0,0)) is shown in Fig. 5.

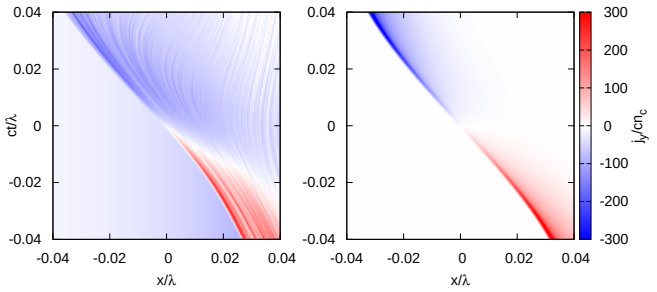

FIG. 10: Transverse current density from the simulation near the SPP (a) and calculated analytically via. (14), $n = 1$ (b). Simulation parameters are the same compared to Fig. 5. The parameters used by the analytical calculation for $x_0(t)$: $\alpha_0 = 1 \cdot 10^4$, $n_\mathrm{m} = 500$ and $\gamma = 2.5$, for shape: $a = 1 \cdot 10^{-3}\lambda$ and $\tilde{\tilde{\sigma}} = 0.02\lambda$. The velocity v is derived from the given gamma factor.

example (parabolic case) the first order gamma spike is obtained. In order to find the parameter ranges which correspond to whip or parabolic case we perform a number of simulations. Using moderate intensity of incident wave ($a_0 = 10$) we vary the steepness of the exponential density gradient as well as incident angle. For each parameter set we consider the reflected radiation. In Fig. 12 we visualized the maximal amplitude of reflected wave for each parameter set respectively. Consider the incident angle between 45 and 60, since by this angles the most interesting things happen. Of corse we notice the sharp increase of the reflected wave amplitude in the area around $\sigma = 0.4\lambda$. We call this area high amplitude parameter set (HAPS). In this area we mostly obtain the second order γ-spikes and the current doesn't change its sign in SPPs like in Fig. 7 Furthermore our study shows that the maximal longitudinal velocity of the certain boundary electron layer increase monotonously with σ until HAPS, where

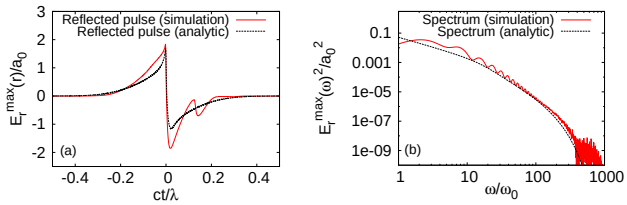

FIG. 11: Reflected radiation obtained from the simulation ((a) red) and from analytical current distribution ((a) black), as well as the corresponding spectra in (b).

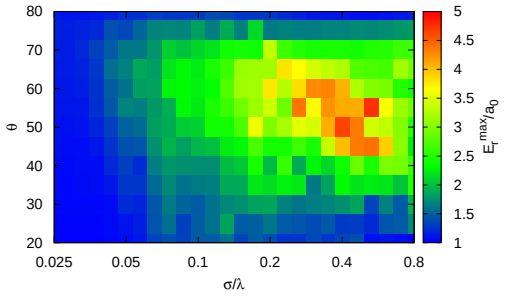

FIG. 12: Each point in these pictures corresponds to the maximal amplitude obtained from the reflected radiation taken from corresponding simulation. We have different angles of incidence along y-axis and different steepness of the density gradient along x-axis, where σ is taken from (1) and $n_0 = 100n_c$ (laboratory frame).

it almost reaches c. For $\sigma < 0.05\lambda$ the boundary oscillates to slowly so that any short pulses are generated. Roughly between 0.05λ and 0.1λ we obtain the reflected radiation similar to Fig. 11. We call this area moderate amplitude parameter set (MAPS). Here we have only first order γ-spikes and the current changes sign in SPPs (Fig. 10). Thus the reflected spectrum in MAPS can be approximated with equation (8) (parabolic case) and the area of HAPS corresponds than to the exponential case (equation (13)). In the area between MAPS and HAPS the interaction is too complicated to be attributed to any model.

CONCLUSION

We could obtain two different analytical expressions of electron density profile describing the density spikes in two different cases. Further we presented some simulation results of HHG, where we could obtain the amplitude increasing in the reflected pulse by the factor of five without using extremely intense incident wave. This was possible after we found optimal parameters for density gradient combined with optimal incident angle. Moreover with some simple assumptions we were able to de-

scribe the distribution of transverse current in vicinity of SPP analytically in both cases. Obtained expressions together with the expressions for electron density gave us the possibility to calculate the spectra that fits the original spectra of back radiated pulse quite good.

Our work basically presents the idea of description of the plasma density considering the electron phase space distribution, but this theory has a potential to grow and to be developed further. In this work we introduced just two application examples of our theory. On the other hand it can become a strong tool in laser plasma analysis in general.

This work has been supported by DFG TR18 and EU FP7 Eucard-2 projects.

[1] V. Yanovsky, V. Chvykov, G. Kalinchenko, P. Rousseau, T. Planchon, T. Matsuoka, A. Maksimchuk, J. Nees, G. Cheriaux, G. Mourou, , and K. Krushelnick, Opt. Express **16**, 2109 (2008).

[2] G. A. Mourou and T. Tajima, Science **331**, 41 (2011).

[3] M. B. Schwab, A. Sävert, O. Jäckel, J. Polz, M. Schnell, T. Rinck, L. Veisz, M. Möller, P. Hansinger, G. G. Paulus, and M. C. Kaluza, Appl. Phys. Lett. **103**, 191118 (2013).

[4] G. Mourou, S. Mironov, E. Khazanov, and A. Sergeev, Eur. Phys. J. Special Topics **223**, 1181 (2014).

[5] C. Thaury, F. Quéré, J. Geindre, A. Levy, T. Ceccotti, P. Monot, M. Bougeard, and F. Réau, Nature Physics **3**, 424 (2007).

[6] F. Quéré, C. Thaury, P. Monot, S. Dobosz, P. Martin, J.-P. Geindre, and P. Audebert, Phys. Rev. Lett. **96**, 125004 (2006).

[7] S. Gordienko, A. Pukhov, O. Shorokhov, and T. Baeva, Phys. Rev. Lett. **93**, 115002 (2004).

[8] T. Baeva, S. Gordienko, and A. Pukhov, Phys. Rev. E **74**, 046404 (2006).

[9] B. Dromey, M. Zepf, A. Gopal, K. Lancaster, M. S. Wei, K. Krushelnick, M. Tatarakis, N. Vakakis, S. Moustaizis, R. Kodama, M. Tampo, C. Stoeckl, R. Clarke, H. Habara, D. Neely, S. Karsch, and P. Norreys, Nat. Phys. **2**, 456–459 (2006).

[10] B. Dromey, S. Kar, C. Bellei, D. C. Carroll, R. J. Clarke, J. S. Green, S. Kneip, K. Markey, S. R. Nagel, P. T. Simpson, L. Willingale, P. McKenna, D. Neely, Z. Najmudin, K. Krushelnick, P. A. Norreys, and M. Zepf, Phys. Rev. Lett. **99**, 085001 (2007).

[11] P. Heissler, R. Hörlein, J. M. Mikhailova, L. Waldecker, P. Tzallas, A. Buck, K. Schmid, C. M. S. Sears, F. Krausz, L. Veisz, M. Zepf, and G. D. Tsakiris, Phys. Rev. Lett. **108**, 235003 (2012).

[12] F. Brunel, Phys. Rev. Lett. **59**, 52–55 (1987).

[13] D. an der Brügge and A. Pukhov, Phys. Plasmas **17**, 033110 (2010).

[14] D. an der Brügge and A. Pukhov, "Theory of attosecond pulses from relativistic surface plasmas," e-print arXiv:physics/1111.4133 (2011).

[15] B. Dromey, M. S. Rykovanov, M. Yeung, R. Horlein, D. Jung, D. C. Gautier, T. Dzelzainis, D. Kiefer, S. Palaniyppan, R. Shah, J. Schreiber, H. Ruhl, J. C. Fernandez, C. L. S. Lewis, M. Zepf, and B. M. Hegelich, Nat. Phys. **8**, 804–808 (2012).

[16] B. Dromey, S. Cousens, S. Rykovanov, M. Yeung, D. Jung, D. C. Gautier, T. Dzelzainis, D. Kiefer, S. Palaniyppan, R. Shah, J. Schreiber, J. C. Fernandez, C. L. S. Lewis, M. Zepf, and B. M. Hegelich, New J. Phys. **15**, 015025 (2013).

[17] M. Yeung, B. Dromey, S. Cousens, T. Dzelzainis, D. Kiefer, J. Schreiber, J. H. Bin, W. Ma, C. Kreuzer, J. Meyerter-Vehn, M. J. V. Streeter, P. S. Foster, S. Rykovanov, and M. Zepf, Phys. Rev. Lett. **122**, 123902 (2014).

[18] A. A. Gonoskov, A. V. Korzhimanov, A. V. Kim, M. Marklund, and A. M. Sergeev1, Phys. Rev. E **84**, 046403 (2011).

[19] S. Gordienko and A. Pukhov, Phys. Plasmas **12**, 043109 (2005).

[20] A. Pukhov, J. Plasma Phys. **61**, 425 (1999).

[21] L. D. Landau and E. M. Lifshitz, *The Classical Theory of Fields* (Pergamon, New York, 1964).

[22] H.-C. Wu, "Jpic and how to make a pic code," e-print arXiv:physics/1104.3163 (2011).